Phase diagram of a model for topological superconducting wires

D. Pérez Daroca [1,2] and A. A. Aligia [3,4,2]

[1]*Gerencia de Investigación y Aplicaciones, Comisión Nacional de Energía Atómica, 1650 San Martín, Buenos Aires, Argentina*
[2]*Consejo Nacional de Investigaciones Científicas y Técnicas, 1025 CABA, Argentina*
[3]*Centro Atómico Bariloche, Comisión Nacional de Energía Atómica, 8400 Bariloche, Argentina*
[4]*Instituto Balseiro, Comisión Nacional de Energía Atómica, 8400 Bariloche, Argentina*

(Received 19 April 2021; revised 21 July 2021; accepted 7 September 2021; published 13 September 2021)

We calculate the phase diagram of a model for topological superconducting wires with local s-wave pairing, spin-orbit coupling $\vec{\lambda}$, and magnetic field $\vec{B}$ with arbitrary orientations. This model is a generalized lattice version of the one proposed by Lutchyn *et al.* [Phys. Rev. Lett. **105**, 077001 (2010)] and Oreg *et al.* [Phys. Rev. Lett. **105**, 177002 (2010)], who considered $\vec{\lambda}$ perpendicular to $\vec{B}$. The model has a topological gapped phase with Majorana zero modes localized at the ends of the wires. We determine analytically the boundary of this phase. When the directions of the spin-orbit coupling and magnetic field are not perpendicular, in addition to the topological phase and the gapped nontopological phase, a gapless superconducting phase appears.

DOI: 10.1103/PhysRevB.104.115125

I. INTRODUCTION

The study of topological superconducting wires, which host Majorana zero modes (MZMs) at their ends, is a field of intense research in condensed matter physics, not only because of the interesting basic physics involved [1], but also because of possible applications in decoherence-free quantum computing [2–5].

In 2010, Lutchyn *et al.* [6] and Oreg *et al.* [7] proposed a model for topological superconducting wires describing a system formed by a semiconducting wire with spin-orbit coupling (SOC) and proximity-induced s-wave superconductivity under an applied magnetic field perpendicular to the direction of the SOC. This yields a topological superconducting phase with MZMs localized at its ends. The observation of these MZMs in these types of wires was reported in different experimental studies [8–11].

The search for different models and mechanisms leading to topological superconducting phases continues being a very active avenue of research theoretically and experimentally.

More recently, there has been experimental research as well as theoretical studies in similar models, including those for time-reversal invariant topological superconductors [12,13], of the effects of MZMs in Josephson junctions, in particular because the dependence on the applied magnetic flux introduces an additional control knob [13–20].

In particular, it has been recently proposed that the current-phase relation measured in Josephson junctions may be used to find the parameters that define the MZMs [20]. A possible difficulty in these experiments is the slow thermalization to the ground state in the presence of a gap [21]. A way to circumvent this problem is to rotate the magnetic field slowly from a direction not perpendicular to the SOC in which the system is in a gapless superconducting phase, in which thermalization is easier [20]. Therefore, it is convenient to know the phase diagram of the system and the extension of this gapless phase.

In this work we calculate the phase diagram of the lattice version of the model and discuss in particular the gapless phase. The paper is organized as follows. In Sec. II we describe the model. The topological invariants use to define the phase diagram are presented in Sec. III. In Sec. IV we show the numerical results, analytical expressions for the boundaries of the topological phase, and discuss briefly the Majorana zero modes. We summarize the results in Sec. V.

II. MODEL

The model for topological superconducting wires studied in this work is the lattice version of that introduced by Lutchyn *et al.* [6] and Oreg *et al.* [7]. The Hamiltonian can be written as [20]

$$H = \sum_{\ell} [\mathbf{c}_{\ell}^{\dagger}(-t\ \sigma_0 - i\vec{\lambda}\cdot\vec{\sigma})\mathbf{c}_{\ell+1} + \Delta c_{\ell\uparrow}^{\dagger} c_{\ell\downarrow}^{\dagger} + \text{H.c.} - \mathbf{c}_{\ell}^{\dagger}(\vec{B}\cdot\vec{\sigma} + \mu\sigma_0)\mathbf{c}_{\ell}], \quad (1)$$

where ℓ labels the sites of a chain, $\mathbf{c}_{\ell} = (c_{\ell\uparrow}, c_{\ell\downarrow})^T$, t is the nearest-neighbor hopping, $\vec{\lambda}$ is the SOC, Δ represents the magnitude of the proximity-induced superconductivity, $\vec{B}$ is the applied magnetic field, and μ is the chemical potential. As usual, the components of the vector $\vec{\sigma} = (\sigma_x, \sigma_y, \sigma_z)$ are the Pauli matrices and σ_0 is the 2×2 unitary matrix. The pairing amplitude Δ can be assumed real. Otherwise, the phase can be eliminated by a gauge transformation in the operators $c_{\ell\sigma}^{\dagger}$ that absorbs the phase.

Without loss of generality, we choose the z direction as that of the magnetic field ($\vec{B} = B\hat{\mathbf{z}}$) and x perpendicular to the plane defined by $\vec{\lambda}$ and $\vec{B}$ ($\vec{\lambda} = \lambda_y\hat{\mathbf{y}} + \lambda_z\hat{\mathbf{z}}$). After Fourier transformation, the Hamiltonian takes the form $H = \sum_k H_k$,

with

$$H_k = -[\mu + 2t\ \cos(k)](c^\dagger_{k\uparrow}c_{k\uparrow} + c^\dagger_{k\downarrow}c_{k\downarrow}) - B(c^\dagger_{k\uparrow}c_{k\uparrow} - c^\dagger_{k\downarrow}c_{k\downarrow}) - 2\ \sin(k)[i\lambda_y(c^\dagger_{k\uparrow}c_{k\downarrow} - c^\dagger_{k\downarrow}c_{k\uparrow}) + \lambda_z(c^\dagger_{k\uparrow}c_{k\uparrow} - c^\dagger_{k\downarrow}c_{k\downarrow})] + \Delta(c^\dagger_{k\uparrow}c^\dagger_{-k\downarrow} + c_{-k\downarrow}c_{k\uparrow}). \quad (2)$$

Using the four-component spinor $(c^\dagger_{k\uparrow}, c^\dagger_{k\downarrow}, c_{-k\uparrow}, c_{-k\downarrow})$ [22], the contribution to the Hamiltonian for wave vector k can be written in the form

$$H_k = -[\mu + 2t\ \cos(k)]\tau_z \otimes \sigma_0 - B\tau_z \otimes \sigma_z - \Delta\tau_y \otimes \sigma_y + 2\lambda_y \sin(k)\tau_z \otimes \sigma_y - 2\lambda_z \sin(k)\tau_0 \otimes \sigma_z, \quad (3)$$

where the Pauli matrices σ_α act on the spin space, while the τ_α act on the particle-hole space. Writing the matrix explicitly, H_k takes the form

$$H_k = \begin{pmatrix} -a - B - z & -iy & 0 & \Delta \\ iy & -a + B + z & -\Delta & 0 \\ 0 & -\Delta & a + B - z & iy \\ \Delta & 0 & -iy & a - B + z \end{pmatrix}, \quad (4)$$

where $a = \mu + 2t\ \cos(k)$, $B = |B| = B_z$, $y = 2\lambda_y \sin(k)$, and $z = 2\lambda_z \sin(k)$.

III. TOPOLOGICAL INVARIANTS

In this section we define the topological invariants we use to characterize the topological phases. In general, the Hamiltonian belongs to topological class D with a $\mathbb{Z}_2$ topological invariant [23,24]. However, for perpendicular $\vec{\lambda}$ and $\vec{B}$ ($z = 0$), the system has a chiral symmetry and belongs to the topological class BDI with a $\mathbb{Z}$ (integer) topological invariant corresponding to a winding number [22]. In this case, the calculation of the topological invariant is simpler, as shown by Tewari and Sau [22].

Following this work, we perform a rotation in $\pi/2$ around the $\hat{y}$ axis in particle-hole space, which transforms τ_z to τ_x: $H'_k = UH_kU^\dagger$ with $U = \exp(-i\pi/4)\tau_y$. With this transformation H'_k becomes

$$H'_k = \begin{pmatrix} -z & 0 & -a - B & \Delta - iy \\ 0 & z & -\Delta + iy & -a + B \\ -a - B & -\Delta - iy & -z & 0 \\ \Delta + iy & -a + B & 0 & z \end{pmatrix}. \quad (5)$$

Taking $z = 0$, this rotation yields an off-diagonal (chiral symmetric) Hamiltonian. This allows us to define a winding number W (a topological $\mathbb{Z}$ invariant) from the phase of the determinant of the 2×2 matrix $A(k)$, which is the upper right corner of Eq. (5) [22]. Specifically $\mathrm{Det}[A(k)] = |\mathrm{Det}[A(k)]|e^{i\theta(k)} = a^2 - B^2 - (\Delta - iy)^2$ and

$$W = \frac{-i}{\pi}\int_0^\pi \frac{d(e^{i\theta(k)})}{e^{i\theta(k)}}. \quad (6)$$

In addition, a $\mathbb{Z}_2$ invariant I can be defined from the relative sign of $\mathrm{Det}(A)$ (which is real for $k = 0$ and $k = \pi$) between the points $k = 0$ and $k = \pi$:

$$I = (-1)^W = \mathrm{sgn}\frac{\mathrm{Det}[A(\pi)]}{\mathrm{Det}[A(0)]}. \quad (7)$$

Looking for the condition that $I \equiv -1 \pmod 2$, we obtain that the conditions for the system to be in the topological phase are that $\lambda_y = |\vec{\lambda}| \neq 0 \neq \Delta$ and the remaining parameters should satisfy

$$|2|t| - r| < |\mu| < |2|t| + r|, \quad \text{with } r = \sqrt{B^2 - \Delta^2} > 0. \quad (8)$$

We note that changing the sign of any of the parameters does not change the boundary of the topological phase. This is due to the symmetry properties of the Hamiltonian [20].

In the more general case, when $\vec{\lambda}$ and $\vec{B}$ are not perpendicular, it is not possible to follow the approach outlined above. In this case, we use the Zak Berry phase to construct the topological invariant [24–34]. Specifically, the Hamiltonian H_k has four different eigenvectors and, for each of them, following Zak [25], one can calculate a Berry phase from the Bloch functions as the wave vector k varies in the loop $0 \leqslant k \leqslant 2\pi$ (with $k = 2\pi$ equivalent to $k = 0$). For each eigenstate $|u(k)\rangle$ of H_k, the Berry phase is

$$\gamma = -\mathrm{Im}\int_0^{2\pi} dk\langle u(k)|\frac{\partial}{\partial k}|u(k)\rangle. \quad (9)$$

In addition (as noted before [20]), choosing a suitable coordinate frame ($\vec{\lambda}\cdot\hat{\mathbf{y}} = \vec{B}\cdot\hat{\mathbf{y}} = 0$), the Hamiltonian Eq. (1) is invariant under an antiunitary operator defined as the product of inversion (defined by the transformation $\ell \leftrightarrow N + 1 - \ell$, for a chain with N sites) and complex conjugation, implying that the Berry phase γ is quantized with only two possible values 0 and π (mod 2π) [31]. Naturally the value of the Berry phase does not depend on the choice of the reference frame. Therefore, as for an insulator, if the system has a gap, the sum of the Berry phases of all one-particle states of energies below the gap mod 2π defines a $\mathbb{Z}_2$ topological number, indicating that the system is trivial (topological) if this sum is equivalent to 0 (π) mod 2π [24,34]. Moreover, from Eq. (3) it is easy to realize that the charge conjugation $c^\dagger_{\ell\sigma} \leftrightarrow c_{\ell\sigma}$, which in Fourier space means $c^\dagger_{k\sigma} = (1/\sqrt{N})\sum_l e^{-ik\ell}c^\dagger_{\ell\sigma} \leftrightarrow c_{-k\sigma}$, transforms $H_k \leftrightarrow -H_{-k}$. Therefore, the sum of the Berry phases of all positive eigenvalues gives the same topological number as the sum of all negative eigenvalues.

In our model, H_k has four eigenvalues $E(k)$. The lowest one $E_1(k)$ is always negative and the corresponding eigenvector has always a Berry phase 0. From the above mentioned charge-transfer symmetry, the fourth eigenvalue (the highest one) has energy $E_4(k) = -E_1(-k) > 0$. Therefore, the Berry phase of the second eigenvalue (which is equal to that of the third one) determines the $\mathbb{Z}_2$ invariant. We have calculated the Berry phase γ of each of the four bands (and particularly the second one) from the normalized eigenvectors $|u_j\rangle = |u(k_j)\rangle$ of the 4×4 matrix obtained numerically at M wave vectors $k_j = 2\pi(j-1)/M$, using a numerically invariant expression [28,33]. This expression is derived in the following way. Discretizing Eq. (9) and approximating

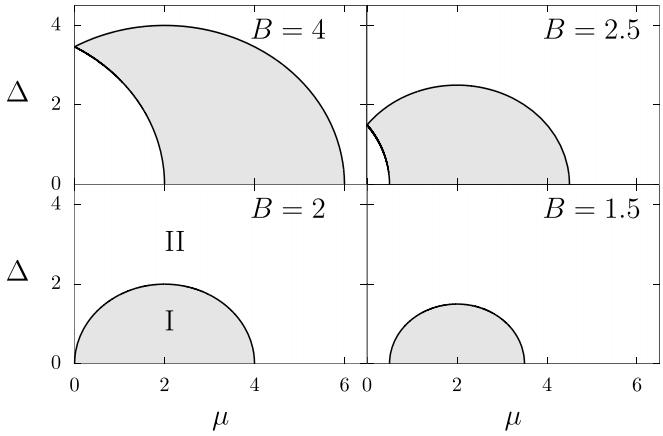

FIG. 1. Phase diagram in the μ, Δ plane for perpendicular $\vec{\lambda}$ and $\vec{B}$, $t = 1$, $\lambda = |\vec{\lambda}| = 2$, and several values of B. Gray region I denotes the topological sector and white region II the nontopological one.

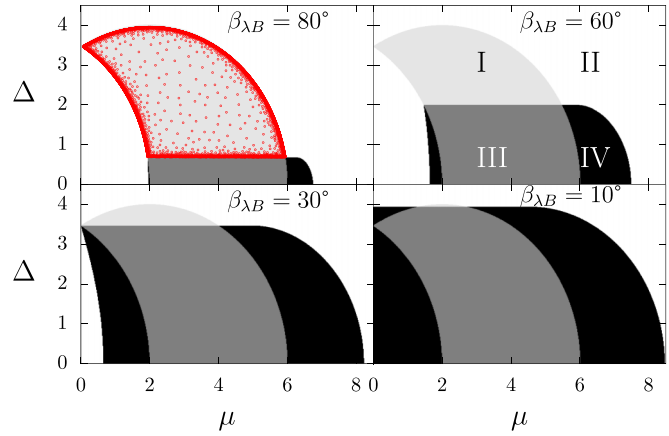

FIG. 2. Phase diagram in the μ, Δ plane for $t = 1$, $\lambda = 2$, $B = 4$, and several values of the angle $\beta_{\lambda B}$ between $\vec{\lambda}$ and $\vec{B}$. Regions I and II as in Fig. 1. Region III (IV) in dark gray (black) corresponds to the gapless phase with Berry phase π (0). The red points at the top left correspond to numerical calculations which detected localized states at the ends.

$\partial|u(k)/\partial k = (M/2\pi)[|u(k_{j+1})\rangle - |u(k_j)\rangle]$, one obtains

$$\gamma = -\mathrm{Im}\sum_{j=1}^{M}[\langle u_j|(|u_{j+1}\rangle - |u_j\rangle)]. \tag{10}$$

If M is large enough so that k_j and k_{j+1} are very close, then $x = \langle u_j|u_{j+1}\rangle - 1$ is very small and one can retain only the first term in the Taylor series expansion $\ln(1+x) = x - x^2/2 + \cdots$. Replacing in Eq. (10) one obtains

$$\gamma = -\mathrm{Im}[\ln(\mathrm{P})],$$
$$\text{where } P = \langle u_1|u_2\rangle\langle u_2|u_3\rangle \ldots \langle u_{M-1}|u_1\rangle. \tag{11}$$

It is easy to see that Eq. (9) is gauge invariant. This means that the result does not change if $|u(k)\rangle$ is replaced by $e^{i\varphi(k)}|u(k)\rangle$, where $\varphi(k)$ is a smooth function with $\varphi(2\pi) = \varphi(0)$. Similarly, the product P is independent of the base chosen by the numerical algorithm to find the eigenstates $|u_j\rangle$. Therefore, Eq. (11) is numerically gauge invariant. Analyzing the change in the results with increasing M, we find that $M \sim 250$ is enough to obtain accurately all phase boundaries shown below. A further increase in M leads to changes that are not visible in the scale of the figures.

This $\mathbb{Z}_2$ topological invariant defined by the Berry phase of the second (or third) state can be trivially extended to the gapless case if the energies of the second and third state do not cross as a function of k. Even if the energies cross the Berry phases can be calculated switching the states at the crossing. However, this case is not of interest here.

IV. RESULTS

A. Phase diagram

We start by discussing the simplest case of perpendicular $\vec{\lambda}$ and $\vec{B}$. In Fig. 1 we display the resulting phase diagram for some parameters, showing the possible different shapes. There are two gapped phases, the trivial (white region II) and the topological one (light gray I), separated in general by two circular arcs defined by Eqs. (8). For simplicity we discuss the case $t, B > 0$. The topological character is independent of the sign of the different parameters. If $B < 2t$, the region of possible values of $|\mu|$ inside the topological sector extends from $2t - B$ to $2t + B$ for $\Delta \to 0$ and shrinks for increasing Δ until it reduces to the point $|\mu| = 2t$ for $\Delta \to B$. If $B = 2t$, the semicircle touches the point $\mu = 0$. For larger B, the region $|\mu| < \sqrt{B^2 - \Delta^2} - 2t$ for $\Delta^2 < B^2 - 4t^2$ is excluded from the topological region.

While for perpendicular $\vec{\lambda}$ and $\vec{B}$, the gap vanishes only at particular lines in the phase diagram (black lines in Fig. 1) for which the topological transition takes place, for general angles $\beta_{\lambda B}$ between both vectors, there is a finite region in the μ, Δ plane for which the gap vanishes, in particular for $|\Delta| < \Delta_c$, where Δ_c is a critical value, independent of μ, determined analytically below. Before presenting the analytical calculation, we describe the general features of each phase in the phase diagram, as shown in Fig. 2. The gapped regions in the figure are denoted by I and II. The remaining two regions are gapless. We separate them by the trivial (topological) character of the Berry phases of the second and third eigenstate, indicating the corresponding regions with black (dark gray) color and roman number IV (III). In spite of the topological Berry phases of the latter gapless phase, MZMs in a finite chain are not expected to be protected against small perturbations because of the absence of a gap. Therefore, we describe this phase as nontopological. Furthermore, we do not find numerically signatures of localized end states in this phase.

We have also checked the boundaries of the topological phase solving numerically finite chains and searching for localized states at their ends and the presence of the finite gap. The localized states are described in Sec. IV D. The presence of the gap is defined by the condition that the determinant $D(k)$ of H_k is positive for each k. As it can be seen in Fig. 2 top left, the results of both approaches agree.

B. Analytical expressions for the boundaries of the topological phase

For perpendicular $\vec{\lambda}$ and $\vec{B}$, the boundaries of the topological phase are defined by Eqs. (8) and the conditions

$|\vec{\lambda}| \neq 0$ and $\Delta \neq 0$. As the angle is changed from 90°, the gap reduces and a nonzero $|\Delta|$ is necessary to keep the gap open (see Fig. 2). For convenience, we discuss first the case $\lambda_z = 0$ (perpendicular $\vec{\lambda}$ and $\vec{B}$) and later consider the general case $\vec{\lambda} = \lambda_y \hat{\mathbf{y}} + \lambda_z \hat{\mathbf{z}}$ with $\lambda_z \neq 0$. For $\lambda_z = 0$, the determinant $D_0(k)$ of H_k [see Eqs. (4) or (5)],

$$D_0(k) = C^2 + 4\Delta^2 y^2,$$
$$C = a^2 + \Delta^2 - B^2 - y^2, \tag{12}$$

is positive semidefinite. It can vanish only for $y = 0$ implying either $k = 0$ or $k = \pi$. For $k = 0$ ($k = \pi$), $C = 0$ implies $|\mu + 2t| = r$ ($|\mu - 2t| = r$). Comparing with Eqs. (8), one realizes that the gap vanishes in general only at one wave vector and only at the transition between topological and nontopological gapped phases, as expected. The exception is the case $|2t| = r$ and $\mu = 0$, for which the gap vanishes at both wave vectors.

In the general case with $z = 2\lambda_z \sin(k)$ nonzero, the determinant of H_k is [see Eq. (5)]

$$D(k) = D_0 + 2z^2(\Delta^2 + y^2 - a^2 - B^2) + z^4. \tag{13}$$

We can consider $D(k)$ as a function of $x = \cos(k)$. For large enough $|\lambda_z|$, it turns out that, at the wave vector $k = 0$, and parameters for which $C = y = z = 0$ [implying $D(0) = 0$], $dD(x)/dx > 0$ and as a consequence for small positive k ($x < 1$) the determinant becomes negative, signaling the instability of the gapped phase. For $\lambda_z = 0$, as in the previous case the derivative is negative, but x cannot be increased beyond 1, so that $D(k) \geqslant 0$. A similar reasoning with the corresponding changes in the sign can be followed for $k = \pi$. An explicit calculation of the derivative using the conditions $C = \sin(k) = 0$ gives

$$\frac{dD}{dx} = 32\left[B^2\lambda_z^2 - \Delta^2\left(\lambda_z^2 + \lambda_y^2\right)\right]x. \tag{14}$$

This implies that to have a gap one needs that $|\Delta| > \Delta_c$, where

$$\Delta_c^2 = B^2 \frac{\lambda_z^2}{\lambda_z^2 + \lambda_y^2} = B^2 \cos^2(\beta_{\lambda B}). \tag{15}$$

This condition has been found before for a model similar to ours in the continuum with quadratic dispersion [35].

After some algebra, the determinant in the general case can be written in the form

$$D = (C - z^2)^2 + 16\left(\lambda_z^2 + \lambda_y^2\right)\left(\Delta^2 - \Delta_c^2\right)(1 - x^2), \tag{16}$$

which is again positive semidefinite for $|\Delta| > \Delta_c$ and positive definite for $0 \neq k \neq \pi$, indicating a gapped phase. Since $x = 1$ implies $y = z = 1$, the remaining boundaries of the topological phase remain the same as for perpendicular $\vec{\lambda}$ and $\vec{B}$. For $|\Delta| = \Delta_c$ (as in Fig. 4), the values of k for which the determinant vanishes are given by the solutions with $|x| \leqslant 1$ of the following quadratic equation:

$$0 = 4(t^2 + \lambda^2)x^2 + 4t\mu x + \mu^2 + \Delta_c^2 - B^2 - 4\lambda^2, \tag{17}$$

where $\lambda = |\vec{\lambda}|$.

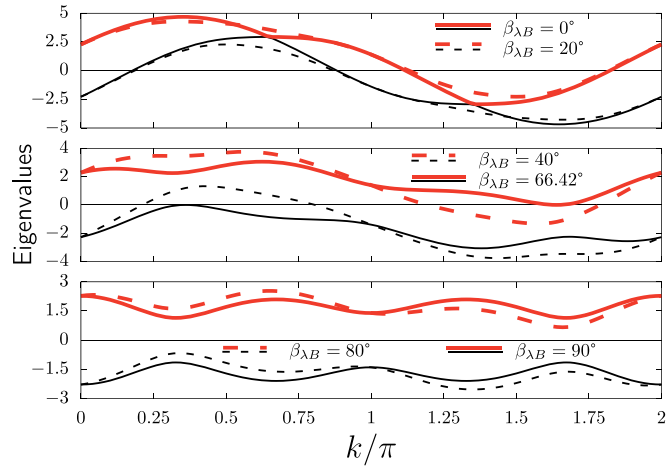

FIG. 3. Second (black thin lines) and third (red thick lines) eigenvalues of H_k as a function of wave vector for $t = 1$, $\lambda = \Delta = 2$, $B = \mu = 5$, and several values of the angle $\beta_{\lambda B}$ between $\vec{\lambda}$ and $\vec{B}$.

C. Transition from the topological phase to the gapless phases

To gain insight into the transition from the topological phase to the gapless phases, we represent in Fig. 3 the second and third eigenvalues of H_k [$E_2(k)$ and $E_3(k)$, respectively] for different values $\beta_{\lambda B}$ of the angle between $\vec{\lambda}$ and $\vec{B}$. The parameters are such that, for $\vec{\lambda} \cdot \vec{B} = 0$, the system is in the topological phase with a finite gap. As the angle is changed (in either direction) the gap between the second and third eigenvalue decreases until at a certain critical angle [given by the solution of Eq. (17)] $E_2(k_c) = E_3(-k_c) = 0$ at one particular wave vector k_c (0.3613π in the figure), denoting the onset of the gapless phase. Further turning $\vec{\lambda}$ and $\vec{B}$ to the parallel (or antiparallel) direction, both eigenvalues vanish at two different wave vectors.

If keeping the other parameters fixed, the chemical potential μ is changed towards one border μ_c of the topological phase for $\vec{\lambda} \cdot \vec{B} = 0$ [given by Eq. (8)]; the critical wave vector k_c is displaced either to $k_c = 0$ or to $k_c = \pi$ depending on the border. This is illustrated in Fig. 4. At the corresponding

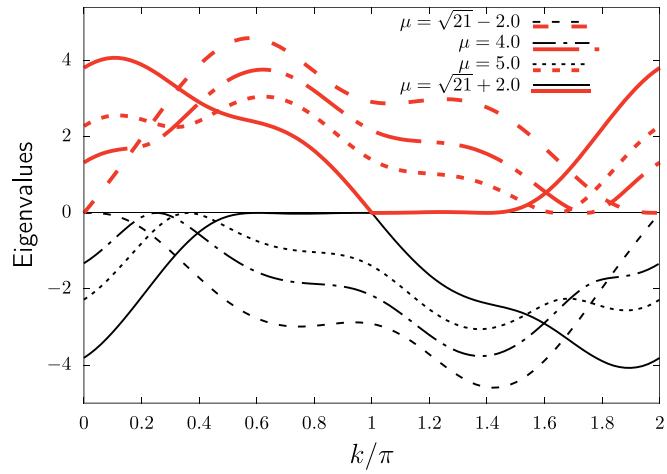

FIG. 4. Same as Fig. 3 for $t = 1$, $\lambda = \Delta = 2$, $B = 5$, $\beta_{\lambda B} = 66.42°$, and several values of μ.

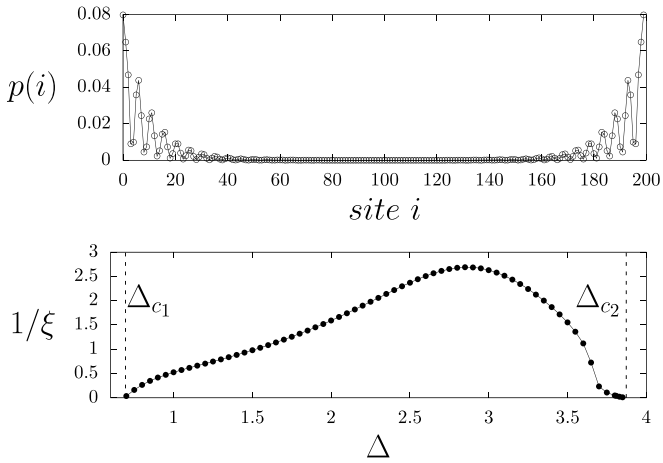

FIG. 5. Top: probability of finding a fermion at each site of a chain for the eigenstate of lowest positive energy for $t = 1$, $\lambda = 2$, $B = 4$, $\beta_{\lambda B} = 80°$, $\mu = 3$, and $\Delta = 0.75$. Bottom: inverse of the localization length as a function of Δ. The transition between phases I and III is at $\Delta_{c_1} = 0.694592711$ and the transition between phases I and II is at $\Delta_{c_2} = 3.872983346$.

border $\mu = \mu_c$, one has $E_2(k_c) = E_3(k_c) = 0$, indicating a crossing of the levels which is also accompanied by a change in the Berry phases of the corresponding eigenvectors. Further displacing μ the system enters the nontopological gapped phase. Therefore, the point $\mu = \mu_c$, $\Delta = \Delta_c$ is at the border of the topological phase, the nontrivial gapless phase with Berry phase π, and the nontopological gapped phase. In fact also the trivial gapless phase reaches this tetracritical point in the phase diagram (see Fig. 2).

D. Majorana modes

The topological phase is characterized by the presence of Majorana modes' zero modes at the ends of an infinite chain. For a finite chain, the modes at both ends mix, giving rise to a fermion Γ and its Hermitian conjugate with energies $\pm E$ which decay exponentially with the length L of the chain. We have obtained Γ numerically in chains of $L \sim 200$ sites. The probability $p(i)$ of finding a fermion at site i (adding both spins and creation and annihilation) is shown in Fig. 5. The main feature of the top figure is a decay of $p(i)$ as the distance from any of the ends increases. We have chosen a case with a rather slow decay to facilitate visualization. In addition to this decay, some oscillations are visible with a short period.

In order to quantify the decay length of the localization of the end modes, we have fit the probability with an exponentially decaying function $p(i) \sim A \exp(-i/\xi)$ at the left end. At the bottom of Fig. 5 we show the dependence of ξ inside the topological phase I as one of the parameters is varied. As expected, ξ diverges at the boundary with the nontopological gapped phase II, which has a different $\mathbb{Z}_2$ topological invariant (at $\Delta_{c_2} = 3.872983346$ in the figure). We also find that ξ diverges at the boundary with the gapless phase III (at $\Delta_{c_1} = 0.694592711$ in the figure), a phase with the same topological invariant but gapless. These facts allow us to obtain numerically the transitions from the localization of the end states (see top left panel of Fig. 2).

V. SUMMARY AND DISCUSSION

Using numerical and analytical methods, we calculate the phase diagram of a widely used model for topological superconducting wires, the essential ingredients of which are local s-wave pairing Δ, spin-orbit coupling $\vec{\lambda}$, and magnetic field $\vec{B}$. We determine the boundary of the gapped topological phase analytically. This phase contains robust Majorana zero modes at both ends that are of great interest. We expect that this result will be relevant for future studies in the field.

The optimal situation for topological superconductivity is when $\vec{B}$ is perpendicular to $\vec{\lambda}$. In this case, both the topological and nontopological phases are gapped. If instead $\vec{B}$ has a component in the direction of $\vec{\lambda}$, a gapless superconducting phase appears for certain parameters. This phase can also be separated in two phases differing in a $\mathbb{Z}_2$ topological invariant. However, due to the absence of a gap, we do not find Majorana zero modes at the ends of the phase with nontrivial $\mathbb{Z}_2$, in contrast to those present in the gapped topological phase.

Tilting the magnetic field to enter the gapless phase might be used as a trick to relax the system to the ground state in some measurements, like Josephson current. In the gapped topological phase, in the absence of low-frequency phonons or other excitations, the physics is dominated by a few bound states inside the gap, completely isolated from the continuum, and the current would oscillate, without reaching a steady state [36]. One way to avoid this problem would be to use a magnetic field so that the system is in the gapless phase, with low-energy excitations available for thermalization, and then rotate adiabatically the field to the desired value so that the system remains in the ground state.

ACKNOWLEDGMENTS

We thank L. Arrachea for helpful discussions. We are sponsored by Grant No. PIP 112-201501-00506 of CONICET, Grants No. PICT-2017-2726, No. PICT-2018-04536, and No. PICT-Raices-2018.

[1] M. Sato and Y. Ando, Topological superconductors: A review, Rep. Prog. Phys. **80**, 076501 (2017).

[2] A. Kitaev, Fault-tolerant quantum computation by anyons, Ann. Phys. (NY) **303**, 2 (2003).

[3] C. Nayak, S. H. Simon, A. Stern, M. Freedman, and S. Das Sarma, Non-Abelian anyons and topological quantum computation, Rev. Mod. Phys. **80**, 1083 (2008).

[4] J. Alicea, New directions in the pursuit of Majorana fermions in solid state systems, Rep. Prog. Phys. **75**, 076501 (2012).

[5] X-J. Liu and A. M. Lobos, Manipulating Majorana fermions in quantum nanowires with broken inversion symmetry, Phys. Rev. B **87**, 060504(R) (2013).

[6] R. M. Lutchyn, J. Sau, and S. Das Sarma, Majorana Fermions and a Topological Phase Transition in Semiconductor-

Superconductor Heterostructures, Phys. Rev. Lett. **105**, 077001 (2010).

[7] Y. Oreg, G. Refael, and F. von Oppen, Helical Liquids and Majorana Bound States in Quantum Wires, Phys. Rev. Lett. **105**, 177002 (2010).

[8] V. Mourik, K. Zuo, S. M. Frolov, S. R. Plissard, E. P. A. M. Bakkers, and L. P. Kouwenhoven, Signatures of Majorana fermions in hybrid superconductor-semiconductor nanowire devices, Science **336**, 1003 (2012).

[9] A. Das, Y. Ronen, Y. Most, Y. Oreg, M. Heiblum, and H. Shtrikman, Zero-bias peaks and splitting in an Al-InAs nanowire topological superconductor as a signature of Majorana fermions, Nat. Phys. **8**, 887 (2012).

[10] S. M. Albrecht, A. P. Higginbotham, M. Madsen, F. Kuemmeth, T. S. Jespersen, J. Nyg, P. Krogstrup, and C. M. Marcus, Exponential protection of zero modes in Majorana islands, Nature (London) **531**, 206 (2016).

[11] M. Deng, S. Vaitiekenas, E. Hansen, J. Danon, M. Leijnse, K. Flensberg, J. Nygård, P. Krogstrup, and C. Marcus, Majorana bound state in a coupled quantum-dot hybrid-nanowire system, Science **354**, 1557 (2016).

[12] A. Haim and Y. Oreg, Time-reversal-invariant topological superconductivity in one and two dimension, Phys. Rep. **825**, 1 (2019).

[13] Y. Volpez, D. Loss, and J. Klinovaja, Time-reversal invariant topological superconductivity in planar Josephson bijunction, Phys. Rev. Research **2**, 023415 (2020).

[14] A. Zazunov, R. Egger, and A. Levy Yeyati, Low-energy theory of transport in Majorana wire junctions, Phys. Rev. B **94**, 014502 (2016).

[15] F. Pientka, A. Keselman, E. Berg, A. Yacoby, A. Stern, and B. I. Halperin, Topological Superconductivity in a Planar Josephson Junction, Phys. Rev. X **7**, 021032 (2017).

[16] M. Hell, M. Leijnse, and K. Flensberg, Two-Dimensional Platform for Networks of Majorana Bound States, Phys. Rev. Lett. **118**, 107701 (2017).

[17] H. Ren, F. Pientka, S. Hart, A. Pierce, M. Kosowsky, L. Lunczer, R. Schlereth, B. Scharf, E. M. Hankiewicz, L. W. Molenkamp, B. I. Halperin, and A. Yacoby, Topological superconductivity in a phase-controlled Josephson junction, Nature (London) **569**, 93 (2019).

[18] A. Fornieri, A. M. Whiticar, F. Setiawan, E. P. Martin, A. C. C. Drachmann, A. Keselman, S. Gronin, C. Thomas, T. Wang, R. Kallaher, G. C. Gardner, E. Berg, M. J. Manfra, A. Stern, C. M. Marcus, and F. Nichele, Evidence of topological superconductivity in planar Josephson junctions, Nature (London) **569**, 89 (2019).

[19] L. Arrachea, A. Camjayi, A. A. Aligia, and L. Gruñeiro, Catalog of Andreev spectra and Josephson effects in structures with time-reversal-invariant topological superconductor wires, Phys. Rev. B **99**, 085431 (2019).

[20] A. A. Aligia, D. Pérez Daroca, and L. Arrachea, Tomography of Zero-Energy End Modes in Topological Superconducting Wires, Phys. Rev. Lett. **125**, 256801 (2020).

[21] N. Bondyopadhaya and D. Roy, Dynamics of hybrid junctions of Majorana wires, Phys. Rev. B **99**, 214514 (2019).

[22] S. Tewari and J. D. Sau, Topological Invariants for Spin-Orbit Coupled Superconductor Nanowires, Phys. Rev. Lett. **109**, 150408 (2012).

[23] A. P. Schnyder, S. Ryu, A. Furusaki, and A. W. W. Ludwig, Classification of topological insulators and superconductors in three spatial dimensions, Phys. Rev. B **78**, 195125 (2008).

[24] S. Ryu, A. P. Schnyder, A. Furusaki, and A. W. W. Ludwig, Topological insulators and superconductors: tenfold way and dimensional hierarchy, New J. Phys. **12**, 065010 (2010).

[25] J. Zak, Berry's Phase for Energy Bands in Solids, Phys. Rev. Lett. **62**, 2747 (1989).

[26] R. D. King-Smith and D. Vanderbilt, Theory of polarization of crystalline solids, Phys. Rev. B **47**, 1651 (1993).

[27] R. Resta and S. Sorella, Many-Body Effects on Polarization and Dynamical Charges in a Partly Covalent Polar Insulator, Phys. Rev. Lett. **74**, 4738 (1995).

[28] G. Ortiz, P. Ordejón, R. M. Martin, and G. Chiappe, Quantum phase transitions involving a change in polarization, Phys. Rev. B **54**, 13515 (1996).

[29] A. A. Aligia, K. Hallberg, C. D. Batista, and G. Ortiz, Phase diagrams from topological transitions: The Hubbard chain with correlated hopping, Phys. Rev. B **61**, 7883 (2000).

[30] A. A. Aligia, K. Hallberg, B. Normand, and A. P. Kampf, Detection of Topological Transitions by Transport Through Molecules and Nanodevices, Phys. Rev. Lett. **93**, 076801 (2004).

[31] Y. Hatsugai, Quantized Berry phases as a local order parameter of a quantum liquid, J. Phys. Soc. Jpn. **75**, 123601 (2006).

[32] A. A. Aligia, A. Anfossi, L. Arrachea, C. Degli Esposti Boschi, A. O. Dobry, C. Gazza, A. Montorsi, F. Ortolani, and M. E. Torio, Incommmensurability and Unconventional Superconductor to Insulator Transition in the Hubbard Model with Bond-Charge Interaction, Phys. Rev. Lett. **99**, 206401 (2007).

[33] S. Deng, G. Ortiz, and L. Viola, Multiband *s*-wave topological superconductors: Role of dimensionality and magnetic field response. Phys. Rev. B **87**, 205414 (2013).

[34] J. C. Budich and E. Ardonne, Equivalent topological invariants for one-dimensional Majorana wires in symmetry class D, Phys. Rev. B **88**, 075419 (2013).

[35] S. Rex and A. Sudbo, Tilting of the magnetic field in Majorana nanowires: Critical angle and zero-energy differential conductance, Phys. Rev. B **90**, 115429 (2014).

[36] S. B. Chung, J. Horowitz, and X-L. Qi, Time-reversal anomaly and Josephson effect in time-reversal-invariant topological superconductors, Phys. Rev. B **88**, 214514 (2013).